

Optimization on Planning of Trajectory and Control of Autonomous Berthing and Unberthing for the Realistic Port Geometry

Yoshiki Miyauchi^{a,*}, Ryohei Sawada^{a,b}, Youhei Akimoto^{c,d}, Naoya Umeda^a and Atsuo Maki^{a,*}

^aDepartment of Naval Architecture and Ocean Engineering, Graduate School of Engineering, Osaka University, 2-1 Yamadaoka, Suita, Osaka 565-0971, Japan

^bNational Maritime Research Institute, 6-38-1, Shinkawa, Mitaka, Tokyo 181-0004, Japan

^cFaculty of Engineering, Information and Systems, University of Tsukuba, 1-1-1 Tennodai, Tsukuba, Ibaraki 305-8573, Japan

^dRIKEN Center for Advanced Intelligence Project, 1-4-1 Nihonbashi, Chuo-ku, Tokyo 103-0027, Japan

ARTICLE INFO

Keywords:

Autonomous Berthing /Unberthing
Trajectory Planning
Optimization
CMA-ES
Collision Avoidance
Ship Domain

ABSTRACT

To realize autonomous shipping, autonomous berthing and unberthing are some of the technical challenges. In the past, numerous research have been done on the optimization of trajectory planning of berthing problems. However, these studies assumed only a simple berth and did not consider obstacles. Optimization of trajectory planning on berthing and unberthing in actual ports must consider the spatial constraints and maintain sufficient distance to obstacles. The main contributions of this study are as follows: (i) a collision avoidance algorithm based on the ship domain which has variable size by the ship speed is proposed, to include the spatial constraints to optimization; (ii) the effect of wind disturbance is taken into account to the trajectory planning to make a feasible trajectory based on the capacity limit of actuators; (iii) showing that the optimization method for berthing is also eligible for the unberthing, which has been almost neglected; (iv) waypoints are included to the optimization process, to make optimization easier on practical applications. The authors tested the proposed method on two existing ports. The proposed method performed well on both the berthing and the unberthing problem and optimized the control input and the trajectory while avoiding collision with the complex obstacles.

1. Introduction

Realizing autonomous ship navigation, autonomous berthing is one of the major technical challenges. Operations such as berthing and unberthing at a narrow fairway are the most stressful for the navigator. This is because “*The difficulty is not only due to the increase in the number of maneuvering measures, but also because the ship is forced to maneuver in a severe surrounding environment, including spatial constraints such as breakwaters and berths, reduced maneuverability due to low-speed navigation, and increased effects of wind and currents.*” (Seta et al., 2004) Thus, berthing and unberthing are relatively difficult than that of navigation of open-sea. Thus automation of these kinds of maneuvering is useful not only from the viewpoint of reducing the operational cost but also from reducing the workload on the navigator.

In solving the online control of the autonomous berthing, it is effective to use the predefined trajectory and control input as a reference for tracking control obtained by the optimization problem. The process to generate the predefined trajectory is called trajectory planning. In this paper, we defined that trajectory as time series of state of the ship, including geometric paths, with some or all dynamic constraints of the ship, by referring to the definition of Vagale et al. (2021): “*path planning is typically defined within purely geometric space, whereas trajectory planning, or trajectory generation, involves geometric paths endowed with temporal prop-*

erties, e.g., to incorporate dynamics.” Trajectory planning is generally difficult to directly apply to the control algorithm due to its computation requirements, which is longer than the computation time required for real-time control. However, when applying real-time control such as PID control or a black box approach such as neural networks, an optimal trajectory can be used as a reference trajectory to configure a feasible control that is optimized in terms of time and other indicators while satisfying constraints based on actuator capacity limitations and maneuverability.

Another application of trajectory planning is the evaluation tool of ship’s actuator’s capability design on berthing. If the trajectory planning tool can sufficiently incorporate the ship’s dynamics, actuator capability, spatial constraints, and external disturbance, the designer of a ship can evaluate the ship’s berthing capability on specific port geometry and wind condition by utilizing the trajectory planning tool. This would be valuable on the design stage of both autonomous and manned ships.

1.1. Related Research

In the past, numerous research have been done on the optimization of trajectory planning and control of berthing problems (Hasegawa and Kitera, 1993; Ahmed, 2015; Maki et al., 2020a,b). However, most of these studies have assumed only a simple straight berth and do not consider surrounding obstacles. To perform berthing and unberthing in actual ports, it is necessary to avoid static obstacles such as bridge piers, berths other than the destination and anchored ships, as well as moving obstacles such as passing ships.

Only a few research have included the complex geomet-

*Corresponding author

Email addresses: yoshiki_miyauchi@naoe.eng.osaka-u.ac.jp (Y. Miyauchi); maki@naoe.eng.osaka-u.ac.jp (A. Maki)

ric constraints of the port to trajectory planning of berthing. Those research have used a two-stage method which combined the path planning using graph search and optimal control problem solver for trajectory generation: optimization of trajectory planning with polygonal constrains which combined the graph-search and convex optimization (Martinsen et al., 2019, 2021); combined the hybrid A* search algorithm as an initial guess to an optimal control problem solver under the external disturbance (Bitar et al., 2020); the combination of lattice-based motion planning and receding horizon improvement (Bergman et al., 2020). They created an initial trajectory using the lattice-based motion planning which transformed the optimal control problem to classical graph search problem. As a second stage, they conducted optimization based improvement of the initial trajectory using receding horizon improvement while the ship maintaining a fixed safe distance to obstacles.

The difference between present work and those similar previous research (Martinsen et al., 2021; Bitar et al., 2020; Bergman et al., 2020) are as follows. First, They have adopted the two-stage method, which translate the problem to graph search problem to obtain an sub-optimal initial guess at the first stage. The Second stage optimize the initial guess with an optimization problem solver. The proposed method is a single-stage method that does not require an initial guess. Second, they used a simplified dynamic model for the subject ship's maneuvering system: azimuth thruster-like thrust vectoring model. The present work assumed a more common configuration: rudder and propeller system with side thrusters. To incorporate this common configuration, more complex maneuvering models are required than previous research. Finally, these research have only considered the constant safety region to the obstacle, whereas the proposed method used dynamic safety region.

Trajectory planning on other kinds of restricted waters have been reported on: global trajectory planning and collision avoidance of an autonomous surface vessel at narrow ferry passage by safety region and collision region around moving and static obstacles with applying the hybrid dynamic window method (Serigstad et al., 2018); Navigation in restricted channels using reinforcement learning was done by Amendola et al. (2020).

On the optimization of berthing and unberthing trajectory, it is important to consider whether the trajectory avoids the obstacle and whether the trajectory is separated from the obstacle by a sufficient distance for safety. The problem of how much distance a ship should keep from obstacles, was investigated by Fujii and Tanaka (1971) in the 1970s as *effective domain*; and followed by Goodwin (1975), which defined *ship domain* as “*the effective area around a ship which a navigator would like to keep free with respect to other ships and stationary objects.*” Since then, various models have been proposed and applied to the collision avoidance method. Szlapczynski and Szlapczynska (2017) provides a comprehensive review of these ship domain models. However, many models did not address the geographical constraints because the ship domain was mainly used to rep-

resents the safe distance between ships. Effective domain at restricted waters was proposed by Yamanouchi and Fujii (1972) based on observation of navigation outside the port of Yokohama, Japan, and showed that in restricted waters, the ship domain is smaller than open seas, which about three-fourths in the longitudinal direction and about half in the width direction. Ship domain based on traffic at strait proposed by Wang and Chin (2016) that is proportional to the ship length and speed. The coefficients are determined based on the Vessel Traffic Information System (VTIS) database of ships transiting the Singapore Strait by using a genetic algorithm. Pietrzykowski (2008) proposed a ship fuzzy domain with the shape of the narrow fairway as a parameter. Hansen et al. (2013) proposed the ship domain on restricted waters based on AIS data measured on the Fehmarnbelt between Denmark and Germany and Jensen et al. (2013) followed that work by estimating the traffic separating scheme's efficiency on the bridge pier of Fehmarnbelt. However, in our literature survey, the ship domain designed to apply to berthing or unberthing problems cannot be found. To approach the berth wall at the terminal phase of berthing, distance to the obstacle will be much smaller than the ship domain stated above. A novel ship domain applicable for berthing is required.

1.2. Objective and Scope

The objective of this study is to include several major factors necessary for applying optimization of trajectory planning on both berthing and unberthing to practical application, such as spatial constraints and external disturbance. Trajectory planning on unberthing has not been focused on previous research compare to berthing; however, it is equally important to realize the fully autonomous ship. The main contributions of this study are as follows: (i) a new collision avoidance algorithm based on the ship domain which has variable size by the ship speed was proposed, to include the spatial constraints to single-stage optimization of trajectory planning with complex maneuvering model; (ii) effect of wind disturbance was taken into account to the trajectory planning to make a feasible trajectory based on the capacity limit of actuators; (iii) showing that the optimization method for berthing is also eligible for the unberthing, which has been almost neglected on the field on trajectory planning; (iv) waypoints are included to the optimization process, to make optimization easier on practical applications. Major environmental conditions related to berthing and unberthing consist of wind, wave, and current. However, disturbance caused by wave and current were neglected in this study, assuming that the vessel enters a port sheltered by breakwaters.

By adding the idea of ship domain to the collision avoidance algorithm, the proposed method enables the search for a trajectory that maintains an appropriate distance from the obstacle. In this study, the obstacle was limited to a static obstacle, but the algorithm can be extended to a dynamic obstacle.

This study extends the study of Maki et al. (2020a) the Co-variance Matrix Adaption Evolution Strategy (CMA-ES) for the optimization process. The study of Maki

et al. (2020a) only assumed a simple trajectory planning on straight line berth, hence the method had several limitations on practical use such as: can not handle multiple, arbitrary shaped berth; safety distance to obstacles was not considered; external disturbance was not considered. Those limitations are addressed in this study. By incorporating both spatial constraints and wind disturbance, the proposed method can use for both reference trajectory generator of autonomous berthing and evaluation tool of ship's design on berthing capability.

The subject ship is a large single-rudder, single-propeller ship with side thrusters, which can berth and unberth without assistance by tug boats. The proposed method requires only the initial and desired end state, control constraints, and spatial constraints of obstacle geometry as computational conditions. To validate the proposed algorithm, we also performed calculations on multiple ports.

The rest of the paper is organized as follows: Section 2 describes the optimization method of trajectory planning and mathematical modeling of maneuver. The optimization method contains the collision avoidance algorithm, which is newly proposed in this study; Section 3 shows the test result on trajectory planning using a newly introduced optimization scheme with a collision avoidance algorithm. Section 3 also describes the geometry of ports which served as test cases; In Section 4, a discussion on the results shown in the previous section and future works are shown; Finally, section 5 concludes the study.

2. Method

In this study, berthing and unberthing are modeled as 3 degrees-of-freedom problem. The coordinate systems are space-fixed system $o_0 - x_0y_0$ and ship-fixed system $o - xy$ which has its origin on midship. The origin of $o_0 - x_0y_0$ was set as the position of midship at designated berthing point or the start point of unberthing, true-north direction as the positive direction of x_0 , east direction as the positive direction of y_0 . Fig. 1 shows the coordinate systems in this study. State vector is $\mathbf{x} = (x_0, u, y_0, v_m, \psi, r)^T \in \mathbb{R}^6$, where u, v_m are the velocity of $o - xy$ system. The vector of control input is $\mathbf{u} = (\delta, n_p, n_{BT}, n_{ST})^T$. $\delta, n_p, n_{BT}, n_{ST}$ represent the rudder angle, the revolution of propeller, the bow thruster and the stern thruster, respectively. The positive direction of the rudder angle was set to the direction in which the heading angle ψ increase by steering, positive rotation of propeller was set to the advancing direction, positive rotation of side thrusters was set to the direction which the induced force work to move the ship to the positive direction of ship-fixed coordinate y .

Wind disturbance was considered as external force ω , which consist by the true wind direction and true wind speed $\omega = (\gamma_T, U_T)^T$. However, due to the ship's maneuver, an apparent wind affects as the actual force acting on the hull. Hence the apparent wind was computed inside the mathematical model of maneuvering. The zero direction of true wind direction γ_T was set to the direction in which the wind

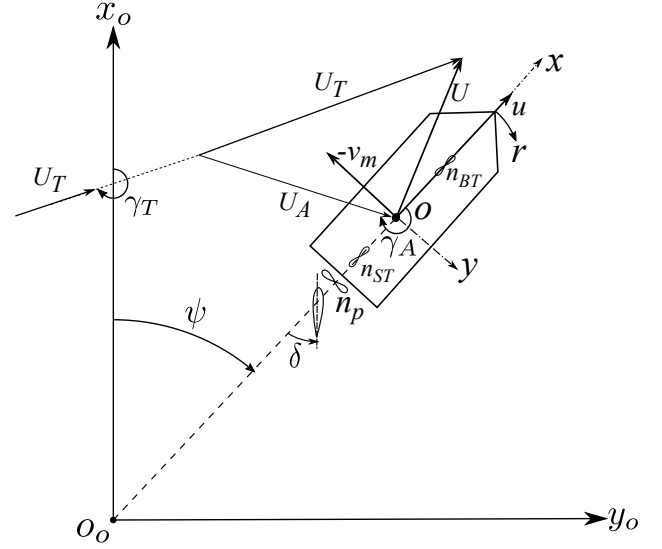


Fig. 1: Coordinate System. The coordinate system consist by space-fixed system $o_0 - x_0y_0$ and ship-fixed system $o - xy$. Notations represent: u, v_m are the velocity of $o - xy$ system; $\delta, n_p, n_{BT}, n_{ST}$ are the rudder angle, the revolution of propeller, the bow thruster and the stern thruster; γ_T, U_T are true wind direction and speed; γ_A, U_A are apparent wind direction and speed.

blows from the positive direction to the negative direction of x_0 .

2.1. Optimization of Trajectory planning

2.1.1. Objective Function

In this study, the berthing and unberthing problems were modeled as time-minimizing problem. Aiming points of the objective function for berthing and unberthing problem are 1) to be collision-free, 2) to satisfy the desired end state, and 3) to minimize the time. Indeed, 1) and 2) are essential constraints that cannot be compromised, but in this study, they are not constraints but included in the objective function. Candidates for evaluation indices other than collision-free and satisfaction of end state can be: minimization of time; minimization of distance; minimization of energy consumption; and ride quality improvement. Regarding those candidates, minimizing time is easy to express in quantitative terms, and minimizing time leads to a short and efficient trajectory. On the other hand, minimizing the distance itself has little practical meaning than minimizing time. Minimizing energy is also not much meaningful since berthing and unberthing account for only a small portion of a ship's energy consumption. The optimization of ride quality is useful for passenger ships, but we avoided it because of the lack of proper quantitative expression of the ride quality.

The state equation shown is Eq. (1):

$$\dot{\mathbf{x}}(t) = \mathbf{f}(\mathbf{x}(t), \mathbf{u}(t), \omega(t)). \quad (1)$$

On the berthing and unberthing problem, the initial and end state are given. By expanding the objective function J proposed by Maki et al. (2020a), J in this study is:

$$J = w_c \cdot C + t_f \cdot \sum_{i=1}^6 w_{\dim,i} \left(x_{\text{tol},i}^2 \mathbf{1}_{\{|x_{\text{des},i} - x_i(t_f)| \leq x_{\text{tol},i}\}} + w_{\text{pen}} (x_{\text{des},i} - x_i(t_f))^2 \mathbf{1}_{\{|x_{\text{des},i} - x_i(t_f)| > x_{\text{tol},i}\}} \right), \quad (2)$$

where the difference $x_{\text{des},5} - x_5(t_f)$ in angle should be treated as a value in $(-\pi, \pi]$ by taking into account the minimum difference angle and $\mathbf{1}_{\{A\}}$ is the indicator function that is 1 if A is true and 0 otherwise. Here, subscript $i = 1, 2, \dots, 6$ means a related term to the i -th component of the state vector. The first term of J is the penalty term for the collision with obstacles, and the second term is for satisfying the desired end state condition. \mathbf{x}_{int} and \mathbf{x}_{des} are the vectors of given initial state and the desired end state. \mathbf{x}_{tol} is the tolerance vector to the difference between the actual and desired end state, which was introduced to prevent t_f from increase due to the pursuit with excessive precision of the end state during the optimization process, same as the previous study (Maki et al., 2020a).

In the case of unberthing, u does not need to be in the certain range of tolerance, instead it should be better just above the certain exit speed. Thus, for the unberthing case, the condition of indicator function of Eq. (2) replaced by $u(t_f) \geq \mathbf{x}_{\text{tol},2}$. w_{pen} is the penalty coefficient when the actual end state not satisfy the \mathbf{x}_{tol} , w_{dim} is the collection vector for state vector components which have different dimensions. On the second term, C is the collision penalty function and w_c is the weight coefficient for collision penalty. Details of collision penalty function is shown on section 2.1.3. List of coefficient and \mathbf{x}_{tol} are shown on Table1.

There is some discussion on how to configure \mathbf{x}_{tol} . On the berthing speed in Japanese ports, Murakami et al. (2015) proposed a regression equation based on measurement. However, their study was conducted from the perspective of allowable values in port design, not from how much the ship needs to slow down. On the heading angle, Roubos et al. (2017) analyzed 555 records of berthing of tankers, bulkers, and container ships in the port of Rotterdam and found that the approach angle to the berth at the moment of impact is less than 1.5° . The tolerance \mathbf{x}_{tol} was set based on the tolerance values of the state at the time of berthing in these previous studies. The velocity component of \mathbf{x}_{tol} was calculated from the regression equation for berthing velocity V which covers 90% of the measured data (Murakami et al., 2015):

$$V = 0.279 \cdot GT^{-0.114}, \quad (3)$$

where GT is the gross tonnage and was assumed as a ferry of approximately 10,000 tons, which operated on the subject port shown on section 3.1. The tolerance of ψ was set to $\mathbf{x}_{\text{tol},5} = 1.0^\circ$, which is slightly smaller than the maximum value in Roubos et al. (2017). The position's tolerance was set to 1.0m, which is small enough for the ship's length.

During the optimization, the optimization method searches for a combination of the time series $\mathbf{u}(t)$ and t_f that minimizes Eq. (2). The time series of the control input is

kept constant during the period of $t_c = 90$ s to prevent frequent input changes and to keep the number of variables to be searched finite. Hence time series of control inputs is discretized into m segments. Thus the variable \mathbf{X} to be optimized is follows:

$$\mathbf{X} \equiv (t_f, \delta_1, \dots, \delta_m, n_{p,1}, \dots, n_{p,m}, n_{BT,1}, \dots, n_{BT,m}, n_{ST,1}, \dots, n_{ST,m})^T \in \mathbf{R}^{4m+1}. \quad (4)$$

In this study $m = 25$, hence the maximum time of simulation is 2250 seconds.

Finally, the optimization problem can be expressed as follows:

$$\begin{aligned} \mathbf{X}_{\text{opt}} &= \text{argmin } J(t_f, \mathbf{u}) \\ \text{subject to : } &x(0) = \mathbf{x}_{\text{int}} \\ &t_{f,\min} \leq t_f \leq t_{f,\max} \\ &|\delta(t)| \leq \delta_{\max} \\ &|n_p(t)| \leq n_{p,\max} \\ &|n_{BT}(t)| \leq n_{BT,\max} \\ &|n_{ST}(t)| \leq n_{ST,\max}. \end{aligned} \quad (5)$$

The optimal trajectory is derived by substituting the optimal solution \mathbf{X}_{opt} to the mathematical model of maneuver. The minimum and maximum value on the exploration domain of \mathbf{X} are shown in Table 2. The limits were set to: the maximum rudder angle of common rudder system; the propeller revolution of advancing at 8 kn; a revolution which can induce the equivalent force of the lateral wind force at 30 m/s when using both of the bow and the stern thruster.

2.1.2. Optimization Method: CMA-ES

As in the previous study (Maki et al., 2020a,b), covariance matrix adaption evolution strategy (CMA-ES) (Hansen, 2006) adapted to box constrains (Sakamoto and Akimoto, 2017) and with restart strategy (Auger and Hansen, 2005) was applied as optimization method. Fig.2 shows the procedure of optimization using CMA-ES. In previous research (Maki et al., 2020a), CMA-ES showed the capability to obtain a feasible solution on optimal berthing problem as a time-minimizing problem while taking into account the collision penalty to berth with simple geometry.

The flow of optimization computation are as follows. Fig. 3 illustrates the flow. First, CMA-ES generated λ candidate solutions $\mathbf{X}_{j=1 \dots \lambda}$ from normal distribution $N(\mathbf{m}^{(i)}, \mathbf{C}^{(i)})$. Second, Generated candidate solutions were evaluated by objective function J (Eq. (2)). To compute J , time history of state vector $\mathbf{x}(t)$ on solution $\mathbf{X}_{j=1 \dots \lambda}$ were computed by numerical simulation using MMG model (Section 2.2). Once the $\mathbf{x}(t)$ for $\mathbf{X}_{j=1 \dots \lambda}$ was obtained, the penalty function C was computed to represent interference between ship domain and obstacles for each solution. Details of C are shown on Section 2.1.3. Third, the $\mathbf{m}^{(i)}$ and $\mathbf{C}^{(i)}$ were updated using weighted average of candidate solutions. Updated parameters are used to generate candidate solutions of next iteration. Candidate solutions were sorted

Table 1
list of weight coefficients and tolerance vectors of end state

Parameter	Value	
Condition	Berthing	Unberthing
\mathbf{x}_{tol}	$(1.0\text{m}, 0.1\text{m/s}, 1.0\text{m}, 0.1\text{m/s}, 1.0^\circ, 0.0764^\circ/\text{s})^\top$	$(1.0\text{m}, 0.0\text{m/s}, 1.0\text{m}, 0.1\text{m/s}, 1.0^\circ, 0.764^\circ/\text{s})^\top$
w_{pen}		1.0×10^4
w_{dim}	$(1/w_L^2, 1/w_U^2, 1/w_L^2, 1/w_U^2, \pi^2, w_L^2/w_U^2)^\top$	
w_C		1.0×10^{10}
w_L		$0.1L_{pp}$
w_U	$\mathbf{x}_{init,2}/2$	$\mathbf{x}_{des,2}/2$

Table 2
Minimum and maximum of end time t_f and control inputs

Parameter	Value
$t_{f,min}$, (s)	630
$t_{f,max}$, (s)	2250
$ \delta_{max} $, (degree)	35
$ n_{p,max} $, (rps)	2.08
$ n_{BT,max} $, (rps)	4.24
$ n_{ST,max} $, (rps)	4.24

in order of J before taking weighted average, to generate better candidate in the next iteration. If the candidate solutions were converged during optimization, The CMA-ES was restarted. On the detail of restart strategy, please see (Maki et al., 2020b). In this study, the initial population size of CMA-ES is 20, and the max size is 240, while the population size was doubled when the restart occurred. Those solution generation-evaluation-update iteration was continued until user defined maximum iteration number was satisfied. The max. iteration number was set to 3×10^5 . And finally, when after the iteration was stopped, optimal solution \mathbf{X}_{opt} was searched from result of iterative process. Again, the optimal trajectory $\mathbf{x}(\mathbf{X}_{opt})$ was derived by feeding \mathbf{X}_{opt} to maneuvering simulation.

2.1.3. Collision avoidance Algorithm

In the previous research (Maki et al., 2020a), collision avoidance was than by adding penalty function C to objective function instead of imposing constraint to system. The penalty function C was defined as the integration of instantaneous penetration length of the vertex of the rectangle surrounding the ship:

$$C = \sum_{i=1}^4 \int_{P_i \in C_{berth}} |Y_i - Y_{berth}| dt, \quad (6)$$

where P_i is the four vertices of the surrounding rectangle, C_{berth} is the area inside the berth, Y_i denotes each y_0 ordinate of P_i and Y_{berth} represents the y_0 coordinate of the berth edge. This collision avoidance method has several limitations for practical use: (a) it can deal with only one berth at a time; (b) the edge of a berth must be parallel to the y_0 direction; (c) safety distance to obstacles, such as berths, breakwaters, buoys or anchoring vessels, is not considered.

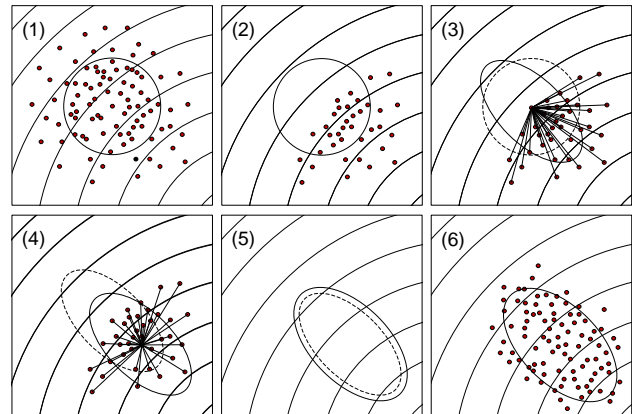


Fig. 2: Schematic presentation of the CMA-ES procedure including (1) generating multiple candidate solutions, (2) evaluating and ranking the solutions based on the objective function, (3) updating the covariance matrix, (4) shifting the center of the distribution to a weighted mean vector, (5) updating the step size and (6) generating multiple candidates in the next step. This figure duplicates Fig. 2 in the literature (Maki et al., 2020b)

The limitation (c): lack of safety distance is the most critical limitation from the practical application perspective. A trajectory which does not maintain safety distance is not suitable for practical use. For instance, when the ship turns, the rectangular points around the ship used in the previous study passed very close to obstacles due to optimize t_f to be the shortest. Such a trajectory may shorten time of berthing, but maneuvering by tracking it may cause discomfort and fear to passengers and nearby manned vessels in practical use. Additionally, the trajectory passing near obstacles is not safe to be used as a reference because there is not enough margin to recover from a gust. Hence, to optimize the trajectory planning in a real port, an optimal trajectory should be searched among trajectories that keep a passing distance away from obstacles as a human captain does.

To overcome these limitations, the authors proposed a new collision avoidance algorithm on this study. The main improvement of the proposed collision avoidance algorithm compared to the previous method stated above as follows: (i) to handle multiple obstacles and arbitrary shape of obstacle (limitation (a) and (b)), both target berth and other obstacles were represented by polygons. (ii) to maintain sufficient

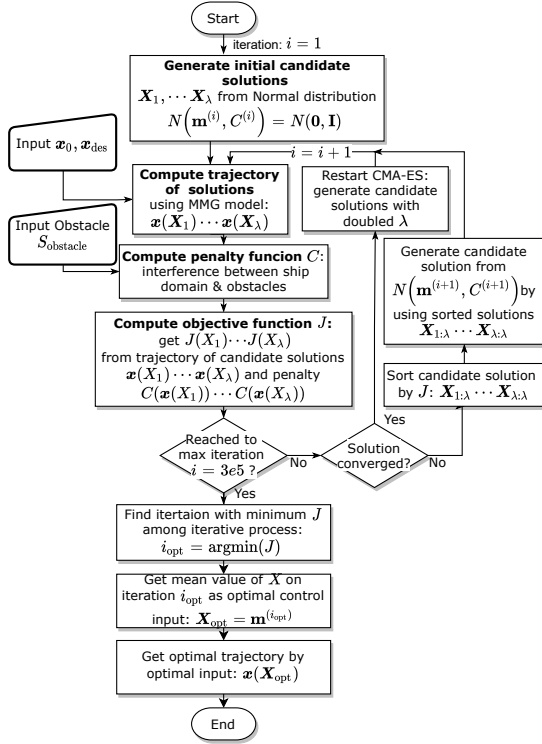


Fig. 3: Flowchart of optimization computation using CMA-ES.

safety distance to the obstacle, the idea of ship domain was introduced to collision avoidance algorithm (limitation (c)).

The key features of proposed method are: (i) the collision avoidance with sufficient safety distance to obstacle done by minimizing the penalty function C which is the interference of ship domain and obstacle; (ii) to simplify the algorithm, ship domain was represented by polygon which has vertices at the boundary of domain (hereinafter, these vertices called as “domain boundary vertices”); (iii) the ship domain varies its size with ship’s speed. This is to enable the ship to maintain distance from obstacle and approach to target berth when the ship reduced its speed; (iv) to generate a favorable gradient of Eq. (2), penalty function C was expressed as integral of instantaneous interference. A favorable gradient is necessary to lead the update process of distribution of candidate solution to be less interfered.

The flow of proposed algorithm avoid are follows. First, the state vector $\mathbf{x}(t)$ for solution \mathbf{X} is fed to collision avoidance algorithm. Second, location of domain boundary vertices $P_{j=1 \dots n_v}$ are computed by $\mathbf{x}(t)$. Third, interference between $P_{j=1 \dots n_v}$ and obstacle polygon $S_{\text{obstacle}, i=1 \dots n_{\text{obstacle}}}$ are computed by Eq. (8) as instantaneous penalty. Finally, sum of $c_{i,j}(t)$ is derived as penalty function C of solution \mathbf{X} and fed to Eq. (2). Note that proposed collision avoidance algorithm are incorporated as a part of optimization process shown on Fig. 3. Details of each part of proposed algorithm are shown below.

The penalty function C was defined as summation of the penetration length of domain boundary vertex to the obstacle

for whole duration of berthing trajectory:

$$C = \int_0^{t_f} \sum_{i=n_{\text{obstacle}}} \sum_{j=n_v} c_{i,j}(t) dt, \quad (7)$$

where $c_{i,j}(t)$ is instantaneous penalty between i -th obstacle polygon $S_{\text{obstacle}, i}$ and j -th domain boundary vertex P_j :

$$c_{i,j}(t) = \begin{cases} L_{\text{penet}, j} & : P_j \in S_{\text{obstacle}, i} \\ 0 & : P_j \notin S_{\text{obstacle}, i} \end{cases}. \quad (8)$$

Here, n_v and n_{obstacle} represents the total number of domain boundary vertices and obstacles, $L_{\text{penet}, i, j}$ is the penetration length of P_j to $S_{\text{obstacle}, i}$, which computed from the length between P_j and nearest edge of $S_{\text{obstacle}, i}$ to P_j .

Details of ship domain Again, in this study, the ship domain was applied to the collision avoidance algorithm. Details of ship domain and domain boundary vertices are shown below. There are two major factors to define the ship domain; the shape of the domain and its size. Regarding the shape of the domain, the shape was designed as an ellipse which has the length ratio of 3:2:1 from midship to the bow, stern, and both sides of a ship, respectively, by referring the research on minimum passing distance in harbor based on inquires to pilots and captains (Inoue et al., 1994).

In terms of the size of the domain, to approach to the berth, the ship domain has to shrink its size to avoid interference between the ship domain and the berth. Moreover, the ship must slow down when maneuvering in the vicinity of obstacle; it is better to keep a longer passing distance due to the increase of minimum stopping distance with speed.

Hence, the P_i ’s coordinate $P_{i,x}$ $P_{i,y}$ are determined by the semi-major axis a , semi-minor axis b and angle α_i :

$$(P_{i,x}, P_{i,y}) = (a \cos \alpha_i, b \sin \alpha_i), \quad (9)$$

where

$$\begin{aligned} a &= L_x(U) + 0.5L_{pp} \\ b &= L_y(U) + 0.5B. \end{aligned} \quad (10)$$

Margin length L_x and L_y are the function of the resultant velocity $U = \sqrt{u^2 + v_m^2}$. Angle α_i is equally spaced, and defined by the ship-fixed coordinate system $o-xy$, with zero in the x direction and positive in the clockwise direction. the x direction margin length L_x has different lengths $L_{x,L} > L_{x,S}$ in front and behind the hull. The length of the long side of the major axis is switched according to the forward speed’s sign:

$$\begin{aligned} u \geq 0 &: \begin{cases} L_{x,L} \leftarrow \alpha_i \in (-\pi/2, \pi/2) \\ L_{x,S} \leftarrow \alpha_i \notin (-\pi/2, \pi/2) \end{cases} \\ u < 0 &: \begin{cases} L_{x,L} \leftarrow \alpha_i \notin (-\pi/2, \pi/2) \\ L_{x,S} \leftarrow \alpha_i \in (-\pi/2, \pi/2) \end{cases} \end{aligned} \quad (11)$$

The $L_{x,L}$, $L_{x,S}$, and L_y were constrained to certain maximum and minimum size to prevent the ship domain from

becoming too large with increasing speed and to maintain a certain passing distance from obstacles even when the speed is low enough. To make the ship domain of this study applicable to the change of geometry of the port, the max. size of the ship domain was determined by the minimum passage width W in the port. This is done by following the idea of dynamic ship domain model of (Liu et al., 2016) which use track width for domain width on the navigation at restricted channels. We assumed a distance of $0.25W$ from the edge of the obstacle in the width direction to pass the head-on situation. Combining with the length ratio of the ellipse's axes, we can obtain:

$$\begin{aligned} L_{x,\max,L} &= 0.75W - 0.5L_{pp} \\ L_{x,\max,S} &= 0.5W - 0.5L_{pp} \\ L_{y,\max} &= 0.25W - 0.5B \end{aligned} \quad (12)$$

On The minimum size, the shape is assumed to be front-to-back symmetric, to maintain sufficient margin on both bow and stern when rotating the ship, which may occur on the terminal phase of berthing and initial phase at confined berth. $L_{y,\min}$ was set to ship's width B , which is a typical stop point before mooring:

$$\begin{aligned} L_{x,\min} &= 0.25L_{pp} \\ L_{y,\min} &= B \end{aligned} \quad (13)$$

Finally, The $L_{x,L}$, $L_{x,S}$, and L_y express as follows:

$$L_{x,L}(U) = \begin{cases} L_{x,\max,L} & : U > U_{\max} \\ L_{x,\min} + \frac{(L_{x,\max,L} - L_{x,\min})(U - U_{\min})}{U_{\max} - U_{\min}} & : U_{\min} \leq U \leq U_{\max} \\ L_{x,\min} & : U < U_{\min} \end{cases} \quad (14)$$

$$L_{x,S}(U) = \begin{cases} L_{x,\max,S} & : U > U_{\max} \\ L_{x,\min} + \frac{(L_{x,\max,S} - L_{x,\min})(U - U_{\min})}{U_{\max} - U_{\min}} & : U_{\min} \leq U \leq U_{\max} \\ L_{x,\min} & : U < U_{\min} \end{cases} \quad (15)$$

$$L_y(U) = \begin{cases} L_y & : U > U_{\max} \\ L_{y,\min} + \frac{(L_{y,\max} - L_{y,\min})(U - U_{\min})}{U_{\max} - U_{\min}} & : U_{\min} \leq U \leq U_{\max} \\ L_{y,\min} & : U < U_{\min} \end{cases}, \quad (16)$$

where linearly changing size with speed over the interval of speed $U \in [U_{\min}, U_{\max}]$. The limits in this study were set to $[U_{\min}, U_{\max}] = [1\text{kn}, 6\text{kn}]$.

Fig. 4 shows the ship domain and domain boundary vertices for $W = 3.08 L_{pp}$, which is the minimum passage width of the port of *Nanko* shown in section 3.1. The number of domain boundary vertices $n_{\text{detect}} = 13$ in this study.

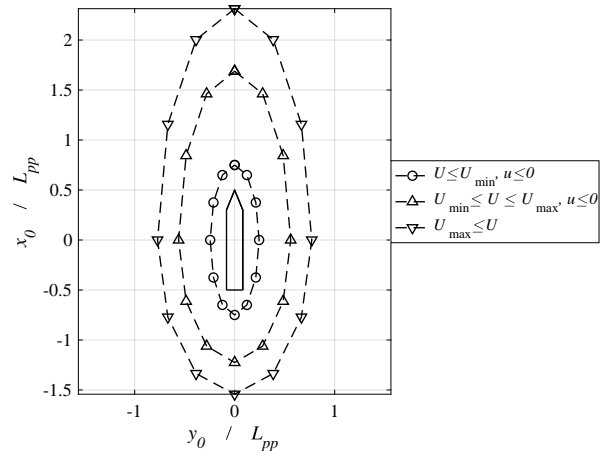


Fig. 4: domain boundary vertices on various speed

2.2. Mathematical Model of Maneuvering

In this section, the mathematical model of ship maneuvering is presented. In this study, the Mathematical Maneuvering Group model (MMG model) (Ogawa and Kasai, 1978; Yasukawa and Yoshimura, 2015) was applied. The MMG model is a mathematical model that is considered to be as related as possible to the physical meaning of hydrodynamics (Ogawa and Kasai, 1978), and one of the most common models for ship maneuvering. The MMG model of the subject ship had been validated with both model ship experiments (Maki et al., 2020b) and full-scale ship trial (Kobayashi et al., 2002).

2.2.1. Subject Ship

The subject ship of this study is the same as previous (Maki et al., 2020a). The subject ship is VLCC M.V. *Esso Osaka*, a single-rudder and single-fixed pitch propeller ship. Although actual *Esso Osaka* does not have any side thruster, to achieve berthing without support from the tug, numerical bow thruster and stern thruster model were added. *Esso Osaka* was chosen because of its availability of the maneuvering model, while the actual ships operated on the subject ports shown on section 3.1 are passenger ferry and RORO cargo ship. These actual ships operated without the assistance of tug during berthing and unberthing and were equipped with side thrusters and a controllable pitch propeller. Although the size was a model scale in the previous study (Maki et al., 2020a), it was expanded to actual ship size. To be equivalent to the ships actually operated on the subject ports, the ship size was shrunken to $L_{pp} = 150$ m while Original *Esso Osaka* is $L_{pp} = 325$ m. The principal particulars of the subject ship are shown in Table 3.

Table 3
Principal particulars of subject ship

Item	Value
Length between perpendicular: L_{pp} (m)	150.0
Ship breadth: B (m)	24.46
Ship draft: d (m)	10.06
Diameter of propeller: D_p (m)	4.20
Area of Rudder: A_R (m ²)	26.58
Diameter of bow thruster: D_{BT} (m)	2.5
Diameter of stern thruster: D_{ST} (m)	2.5
Mass: m (ton)	31,412
Longitudinal center of gravity: x_G (m)	4.75
Transverse projected area: A_T (m ²)	213.55
Lateral projected area: A_L (m ²)	1150.50
Block coefficient: C_b	0.831

2.2.2. MMG model

The 3-DoF equation of motion of MMG model is express as follows:

$$\begin{aligned}
 (m + m_x)\dot{u} - (m + m_y)v_m r - x_G m r^2 &= F_x \\
 (m + m_x)\dot{v}_m - (m + m_y)ur + x_G m \dot{r} &= F_y \\
 (I_{zz} + J_{zz} + x_G^2 m)\dot{r} - x_G m(\dot{v}_m + ur) &= M_N
 \end{aligned} \quad (17)$$

with

$$\begin{aligned}
 F_x &= X_H + X_P + X_R + X_A \\
 F_y &= Y_H + Y_P + Y_R + Y_{SS} + Y_A \\
 M_N &= N_H + N_P + N_R + N_{SS} + N_A
 \end{aligned} \quad (18)$$

Since the MMG model decomposes the hydrodynamic force acting on the ship to sub-model for major components consisting of the ship, the right-hand side of Eq. (18) represents the force or moment acting on each component of the ship; the subscripts H, P, R, A and SS denote the hull, the propeller, the rudder, the external forces by wind and the side thrusters, respectively. Each sub-model contains model coefficients to estimate force form input \mathbf{u} and state \mathbf{x} . The model coefficients, also known as hydrodynamic coefficients, are vessel-specific, and they may vary by the scale of the ship; due to the large discrepancy of the Reynolds number between a scale model for towing tank experiments and the actual ship. However, in this study, model coefficients obtained by scale model test ((Hachii, 2004; Kobayashi et al., 2002) were used, because the values for $L_{pp} = 150$ m of *Esso Osaka* are unknown.

Choice of sub-model follows the previous research (Maki et al., 2020a), with several new additions. For the force acting on the hull, Yoshimura's unified model (Yoshimura et al., 2009) was applied. For the force induced by the propeller, the model is switched based on the operating condition of the propeller. For the propeller forward rotation ($n_p \geq 0$), thrust force X_p expressed by standard MMG model (Yasukawa and Yoshimura, 2015). For the propeller reversal condition ($n_p < 0$), propeller force and moment are modeled by a polynomial equation based on towing tank experiment (Hachii, 2004; Ueno et al., 2001).

For the force induced by rudder, standrd MMG model was applied for forwarding ($u \geq 0$) condition and 4th quadrant operation ($u < 0, n_p < 0$), Kitagawa's model (Kitagawa et al., 2015) for 3rd quadrant operation ($u < 0, n_p \geq 0$). Refer Miyauchi et al. (2021) for the detail of the MMG model used in this paper.

Regarding the external force induced by wind disturbance, Fujiwara's regression formulae (Fujiwara et al., 1998) was used to estimate the wind pressure coefficients:

$$\begin{aligned}
 X_A &= (1/2)\rho_A U_A^2 A_T \cdot C_X \\
 Y_A &= (1/2)\rho_A U_A^2 A_L \cdot C_Y \\
 N_A &= (1/2)\rho_A U_A^2 A_L L_{OA} \cdot C_N,
 \end{aligned} \quad (19)$$

where

$$\begin{aligned}
 C_X &= X_0 + X_1 \cos(2\pi - \gamma_A) + X_3 \cos 3(2\pi - \gamma_A) \\
 &\quad + X_5 \cos 5(2\pi - \gamma_A) \\
 C_Y &= Y_1 \sin(2\pi - \gamma_A) + Y_3 \sin 3(2\pi - \gamma_A) \\
 &\quad + Y_5 \sin 5(2\pi - \gamma_A) \\
 C_N &= N_1 \sin(2\pi - \gamma_A) + N_2 \sin 2(2\pi - \gamma_A) \\
 &\quad + N_3 \sin 3(2\pi - \gamma_A),
 \end{aligned} \quad (20)$$

ρ_A is the density of air, A_T, A_L, L_{OA} are the transverse projected area, the lateral projected area, and the overall length of the ship, respectively. X_i, Y_i, N_i are coefficients to express wind pressure coefficients derived by the regression formulae, which use geometric parameters of the ship as explanatory variables and based on wind tunnel experiment data of numerous scaled ship models.

For the side thruster model, Kobayashi's model (Kobayashi, 1988, 1990) was used, which follows

$$\begin{aligned}
 X_{ST} &= 0 \\
 Y_{SS} &= (1 + a_{YSB} \cdot |\text{Fr}|) \cdot T_{BT} \\
 &\quad + (1 + a_{YST} \cdot |\text{Fr}|) \cdot T_{ST} \\
 N_{SS} &= (1 + a_{NSB} \cdot |\text{Fr}|) \cdot T_{BT} \cdot x_{BT} \\
 &\quad + (1 + a_{NST} \cdot |\text{Fr}|) \cdot T_{ST} \cdot x_{ST} \\
 T_{BT} &= \rho D_{BT}^4 n_{BT}^2 K_{TBT} \\
 T_{ST} &= \rho D_{ST}^4 n_{ST}^2 K_{TST}
 \end{aligned} \quad (21)$$

Here, $a_{YBT}, a_{NBT}, a_{YST}, a_{NST}$ are the coefficients expressing the interaction between hull and thruster. x_{BT}, x_{ST} are the longitudinal location of side thruster. In addition to the interaction effect, the thrust of side thrusters are zero when the longitudinal speed is larger than the threshold: $|u| > u_{\text{threshold}}$. The value of threshold $u_{\text{threshold}} = 2.5722$ (m/s) is equivalent to 5 knots in this study.

3. Computation Results

3.1. Port Geometry

Two ports in Japanese waters were selected for computation; Port of *Nanko* at Osaka bay and the port of *Ariake*

Table 4
Computation condition of port of *Nanko*

Parameter	Value
Condition	Berthing
\mathbf{x}_{int}	$(-598.7 \text{ m}, 8.0 \text{ kn}, -1845.2 \text{ m}, 0.0 \text{ m/s}, 132^\circ, 0.0^\circ/\text{s})^T$
\mathbf{x}_{des}	$(0.0\text{m}, 0.0\text{kn}, 0.0\text{m}, 0.0\text{m/s}, 227^\circ, 0.0^\circ/\text{s})^T$
Condition	UnBerthing
\mathbf{x}_{int}	$(0.0 \text{ m}, 0.0 \text{ kn}, 0.0 \text{ m}, 0.0 \text{ m/s}, 227^\circ, 0.0^\circ/\text{s})^T$
\mathbf{x}_{des}	$(-598.7 \text{ m}, 6.0 \text{ kn}, -1845.2 \text{ m}, 0.0 \text{ m/s}, 312^\circ, 0.0^\circ/\text{s})^T$

Table 5
Computation condition of port of *Ariake*

Parameter	Value
Condition	Berthing
\mathbf{x}_{int}	$(-891.3 \text{ m}, 8.0 \text{ kn}, 3317.5 \text{ m}, 0.0 \text{ m/s}, 326^\circ, 0.0^\circ/\text{s})^T$
\mathbf{x}_{des}	$(0.0\text{m}, 0.0\text{kn}, 0.0\text{m}, 0.0\text{m/s}, 146^\circ, 0.0^\circ/\text{s})^T$
Condition	UnBerthing
\mathbf{x}_{int}	$(0.0 \text{ m}, 0.0 \text{ kn}, 0.0 \text{ m}, 0.0 \text{ m/s}, 146^\circ, 0.0^\circ/\text{s})^T$
\mathbf{x}_{des}	$(-891.3 \text{ m}, 6.0 \text{ kn}, -3317.5 \text{ m}, 0.0 \text{ m/s}, 146^\circ, 0.0^\circ/\text{s})^T$

at Tokyo bay. *Nanko* is the primary port in this study, while *Ariake* is alternate to verify the applicability to arbitrary port geometry of the present method. Overview of ports is shown in Fig. 5 and Fig. 6. These figures also show the start points and the endpoints of berthing. Table 4 and Table 5 show the detailed value of \mathbf{x}_{int} and \mathbf{x}_{des} of computation. As stated in the section 2, the origin of $O_0 - x_0y_0$ coordinates system is set to the endpoint for berthing and the start point for unberthing. The start point of berthing was set just outside the breakwaters of the port. This is because, outside the breakwater, the spatial constrain is not severe as inside; hence the appropriate collision avoidance method might differ. The endpoint was set at the point which perpendicular distance is 40 m from berth wall; Approximately 1.0 B from the broadside of the ship. The berthing condition is the starboard side, head out at *Nanko* and port side, head out at *Ariake*. Note that the obstacle polygons include certain water surfaces at the vicinity of the breakwater as a restricted area.

Both ports have characteristics to make berthing and unberthing difficult: dead end, confined berth which ship necessary to turn 180 degrees, require several course change during navigation, and obstacle landfills that exclude the intended berth. The case of *Nanko* also has a moored vessel near the berthing point as an obstacle. Generally, the ship must comply with the international and local traffic rules; the ship must navigate in the designated passage in a port (for the regulation on the port of *Nanko*, see The Harbor Information Center for the Security of Ship Navigation (2020)). However, in this study, regulatory requirements such as passage and fairway are not considered.

The minimum passage width W , which is the design parameter of domain boundary vertices, are $3.08 L_{\text{pp}}$ for *Nanko* and $2.40 L_{\text{pp}}$ for *Ariake*, respectively.

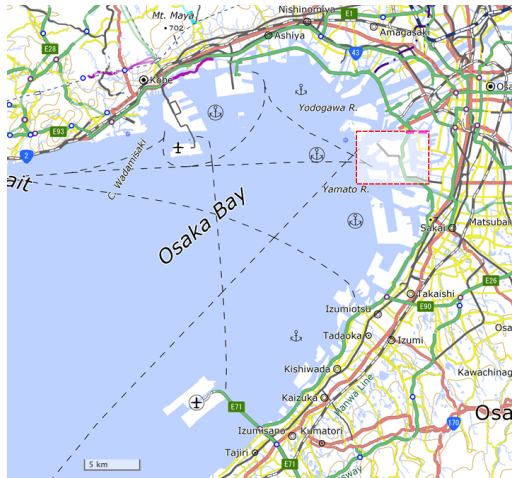
3.2. Berthing and Unberthing Results with proposed ship domain and collision avoidance algorithm

The trajectory planning of berthing and unberthing are conducted with newly introduced objective function including collision avoidance to the polygonal constraints on the port of *Nanko*. The convergence process in the optimization is shown in Fig. 7. The upper-left shows the best objective function J at each iteration. The upper-right shows the difference of J at each iteration and the minimum value of J through the optimization process. The lower-left and lower-right show the square root of the eigenvalue of the covariance matrix and the square root of the diagonal elements of the covariance matrix during the process, respectively. As stated in Maki et al. (2020b), the square root of each eigenvalue represents the axis length of the equidensity ellipsoid, whereas the square root of each diagonal element stands for the standard deviation in each coordinate. From the upper two sub-figures on Fig. 7, J shows impulse-like increases caused by the restart of CMA-ES. By using the restart strategy, CMA-ES let the J converge to several different local minima and choose the best solution from those. In the case of Fig. 7, the optimum solution is obtained at the 94000th iteration. In general, the convergence speed will vary by the computation conditions. However, the maximum iteration number of optimization processes was set to 3×10^5 based on the convergence of Fig. 7, which occur several restarting and obtain local minima. The computation was conducted on the workstation equipped with Intel Xeon Gold 6248R for CPU as a serial computation. The computation time took few days to reach maximum iteration number 3×10^5 .

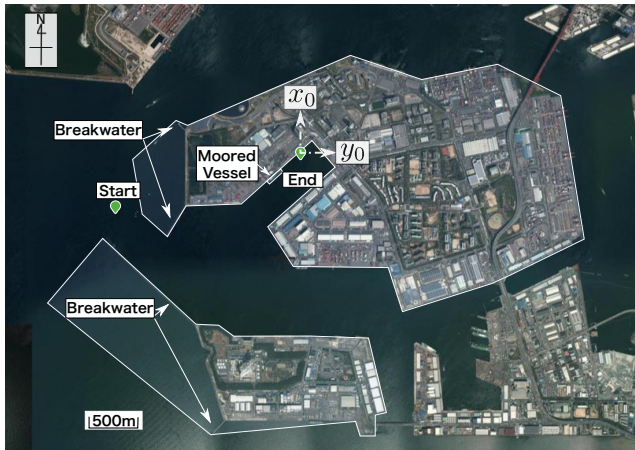
Since CMA-ES is based on a stochastic method, results will differ by the random seed. Table 6 show the t_f , J and C of 10 independent trials on berthing computation of *Nanko* without wind disturbance. From the table, we can find the values of C are zero for all 10 trails. This means, not only

Table 6
Statistical analysis data for J and t_f in 10 trials

: Minimum, Maximum, Quartiles, Mean, and Standard deviation.							
	min	max	Q_1	Q_2	Q_3	Mean	σ
t_f	1081.6	1177.1	1086.5	1098.2	1103.4	1106.0	29.3
J	18.077	19.673	18.159	18.355	18.407	18.484	0.490
$w_c \cdot C$	0.0	0.0	0.0	0.0	0.0	0.0	0.0



(a) Far view; red dashed line rectangular shows the area of the figure below

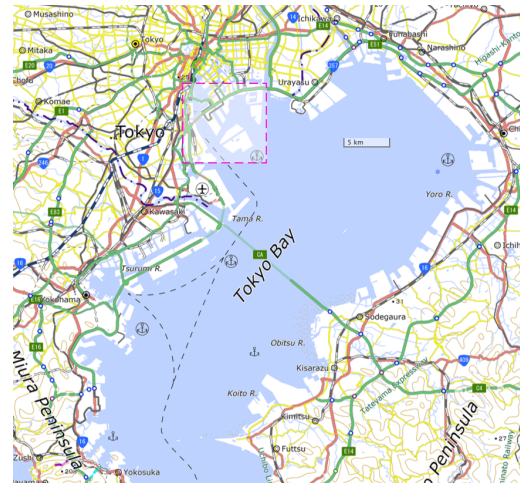


(b) Near view. polygons with white line represent the obstacles which modeled in the computation.

Fig. 5: Port of *Nanko*. Created by Authors based on 1:1,000,000 INTERNATIONAL MAP data and seamless photo data (Geospatial Information Authority of Japan) (<http://maps.gsi.go.jp/>)

collision occurred, but also berthing was conducted with sufficient distance to obstacle by maintaining ship domain. With the newly introduced collision avoidance algorithm, collision avoidance to the obstacle of realistic port geometry was successfully achieved.

Fig. 8 shows the obtained control input $u(t)$ and state $x(t)$ achieved by the optimal $u(t)$ on berthing of *Nanko* without wind disturbance; $U_T = 0$. Note that if $u > u_{\text{threshold}}$, which means thrust of side thrusters are zero, shown as $n_{BT} = 0$



(a) Far view; red dashed line rectangular shows the area of the figure below



(b) Near view. polygons with white line represent the obstacles which modeled in the computation.

Fig. 6: Port of *Ariake*. Created by Authors based on 1:1,000,000 INTERNATIONAL MAP data and seamless photo data (Geospatial Information Authority of Japan) (<http://maps.gsi.go.jp/>)

and $n_{ST} = 0$ in the figure.

Additionally, a comparison computation with the previous method (Maki et al., 2020a) is shown in the figure to show the effectiveness of the proposed method to maintain safety. In the previous study, circumscribed rectangular without safety distance was used to represent the ship's hull. For the comparison computation, the objective function of Maki et al. (2020a) was modified by introducing the collection vector w_{dim} and $w_c = 100$ was used.

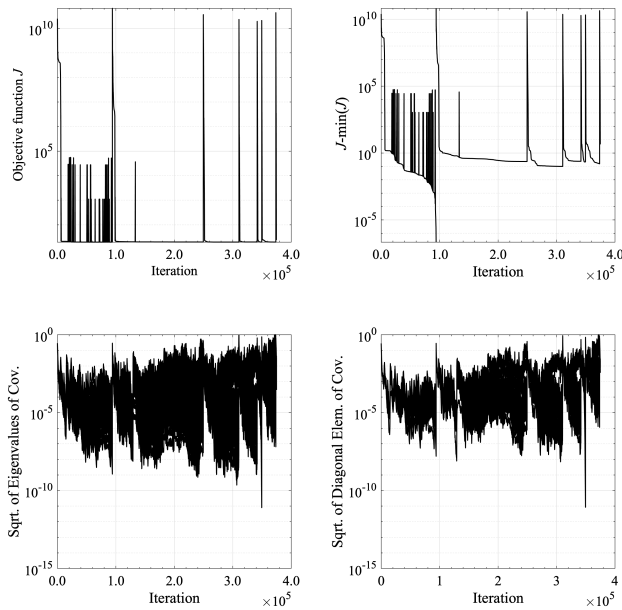


Fig. 7: Optimization process of CMA-ES.

Fig. 8 indicates that the optimization on trajectory planning with the new collision avoidance algorithm works well; the ship has reached the berthing point while avoiding the static obstacles with sufficient distance. Fig. 9 shows the terminal phase of the same berthing result with Fig. 8; Trajectory and control input are shown only for times when the Euclidean distance between midship and berthing point is less than $2L_{pp}$. In Fig. 8 and 9, the light blue ellipses around the ship are ship domain, which shown from $t = 0$ to $t = t_f$ at the intervals of 200 seconds. Fig. 9 also shows the domain boundary vertices themselves. As shown in Maki et al. (2020b), the subject ship tended to turn starboard while propeller reversal. It seems the CMA-ES found the solution which uses the characteristic on the reverse maneuvering of the subject ship to stop within the minimum time.

Figs. 8 and 9 also show the result of comparison computation with the previous method; however, the previous method shows an inappropriate path. The ship got too close to the obstacle when turning the vicinity of the obstacle (Fig. 8) and passing by the moored vessel (Fig. 9). It should be emphasized that the previous method obtained a collision-free trajectory, which means obtained trajectory is optimal from an optimization scheme standpoint; however, it is insufficient for practical use. In contrast, the proposed method can obtain a trajectory with a certain safety distance suitable for practical use.

Fig.10 shows the result of the unberthing computation. Same as berthing, CMA-ES with the proposed collision avoidance algorithm can obtain resalable trajectory and control inputs.

Table7 shows the difference between the desired and the obtained end state: $\mathbf{x}_{des} - \mathbf{x}(t_f)$ and t_f for both of berthing and unberthing. For the berthing, $\mathbf{x}(t_f)$ just fits within the \mathbf{x}_{tol} . This is because objective function did not change when

$\mathbf{x}(t_f)$ was within the range of \mathbf{x}_{tol} , while CMA-ES tried to optimize by shortening the t_f . Meanwhile, in the unberthing computation, $x_{des,2} - x_2(t_f) < 0$ which means the $u(t_f)$ is faster than the desired exit speed, while other state satisfy \mathbf{x}_{tol} .

3.3. Result with Wind Disturbance

Generally, during the berthing and unberthing, the wind disturbance makes it difficult to control a vessel. Hence, the effect of wind must be included in the optimization of trajectory planning. Moreover, the wind has a critical effect on control a ship at the terminal phase of berthing because the thrusts of actuators are kept low, and the distance to berth is small while the ship drifted by the wind. Obviously, the wind speed and direction are unsteady, and instantaneous velocity can only be described by stochastic approach. Hence, it is not appropriate to implement unsteady wind directly to optimization because CMA-ES would optimize while knowing the time series of instantaneous wind due to its iterative process. Nevertheless, including *steady* wind disturbance is meaningful because considering severe conditions by wind disturbance, the obtained trajectory will be a more generous one that takes into account the limits of actuators. In addition to that, by increasing the wind speed, we can find the nominal wind speed limit of a certain ship and spatial constraints of the port.

Under the ideas discussed above, calculations with wind disturbance were conducted for both berthing and unberthing at *Nanko*. Fig.11, 12 show the berthing and unberthing results under wind disturbance of $\omega = (137^\circ, 15 \text{ m/s})$; the true wind direction γ_T is perpendicular to the berth, which pushes the ship towards berth wall. From the figures, we can see that the CMA-ES can obtain a reasonable trajectory even under the wind disturbance when the actuator is capable enough.

3.4. Verification on Different Port Geometry

To show that the proposed method is applicable to multiple ports, it is necessary to verify the method on ports other than *Nanko*, used in the previous section. *Ariake* has the same spatial constraints characteristics while the travel distance is slightly longer than *Nanko* and berthing to the port side. Fig.13 and Fig.14 show the results, which seem reasonable. From the results, we can see that the proposed method is appreciable to different kinds of ports.

3.5. Trajectory Planning Optimization with Waypoints

As shown in the previous section, the proposed method was able to find an appropriate trajectory even under the constraint of complex port geometry. However, it was found that the proposed method does not provide a reasonable solution within the iteration limit when the ship starts from a position far from the breakwaters at the entrance of the port and the initial heading does not point to the entrance of the port. Fig. 15 shows one of the results of such cases, only the local minimum solution that the t_f ends early while advance speed u remain large, was obtained. We assumed that this

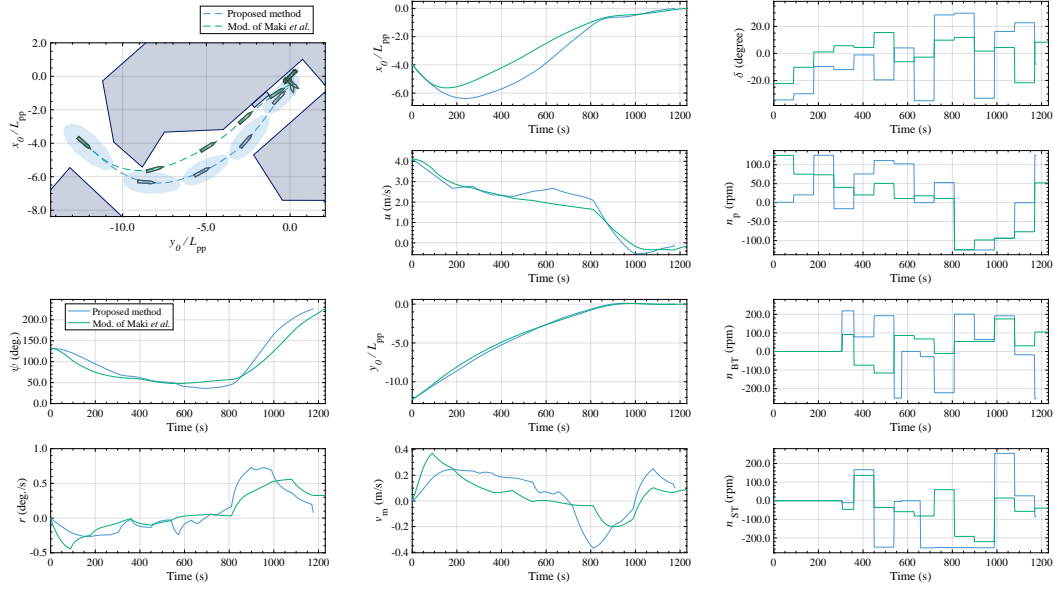


Fig. 8: Optimal control inputs and achieved state of berthing on port of *Nanko*. Ellipses shown in light blue on figure of trajectory at upper left are the ship domains used in collision avoidance algorithm. Comparison computation by the previous study (Maki et al., 2020a) with modification is also shown. The proposed method maintain distance from obstacle when turning while previous method passed without safety distance.

Table 7
Computation results of berthing and unberthing.

parameter	value
Condition	<i>Nanko</i> , berthing, $U_T = 0$
$\mathbf{x}_{des,i} - \mathbf{x}_i(t_f)$	$(1.0\text{m}, 0.1\text{m/s}, -1.0\text{m}, -0.1\text{m/s}, 1.0^\circ, -0.0764^\circ/\text{s})^\top$
$t_f(s)$	1177.1
Condition	<i>Nanko</i> , unberthing, $U_T = 0$
$\mathbf{x}_{des,i} - \mathbf{x}_i(t_f)$	$(1.0\text{m}, -0.2\text{m/s}, -1.0\text{m}, 0.02\text{m/s}, -1.0^\circ, -0.0343^\circ/\text{s})^\top$
$t_f(s)$	994.0

was because: solution exploration not proceed to solutions that navigate to the entrance of port, because the gradient of increasing J occur around the solution toward the opening of the breakwater, due to the small choice of control inputs which can enter to the opening of the breakwater, and surrounding solutions of the favorable solution have significantly large J caused by penalty of collision to breakwaters; a solution that goes straight forward from the initial heading is likely to occur, even if the rudder angle is searched randomly. This is because to change the course of a ship, the rudder angle needs to maintain a certain period until the maneuver develops.

To obtain reasonable solutions of trajectory planning regardless of choice of the initial condition, we tried to generate favorable gradient of the objective function of Eq. (2) when searching the solution around the entrance of port, by including the waypoint portion to J . The J shown on Eq. (2)

was modified to include the component of waypoints J_{WP} :

$$J = (J_1 + J_{WP}) \cdot t_f + w_c C, \quad (22)$$

where

$$J_1 = \sum_{i=1}^6 w_{dim,i} \left(x_{tol,i}^2 \mathbf{1}_{\{|x_{des,i} - x_i(t_f)| \leq x_{tol,i}\}} + w_{pen} (x_{des,i} - x_i(t_f))^2 \mathbf{1}_{\{|x_{des,i} - x_i(t_f)| > x_{tol,i}\}} \right), \quad (23)$$

$$J_{WP} = \sum_{n_{WP}} x_{dim,1} \left(L_{tol}^2 \mathbf{1}_{\{L_{WP,i} \leq L_{tol}\}} + L_{WP,i}^2 \mathbf{1}_{\{L_{WP,i} > L_{tol}\}} \right), \quad (24)$$

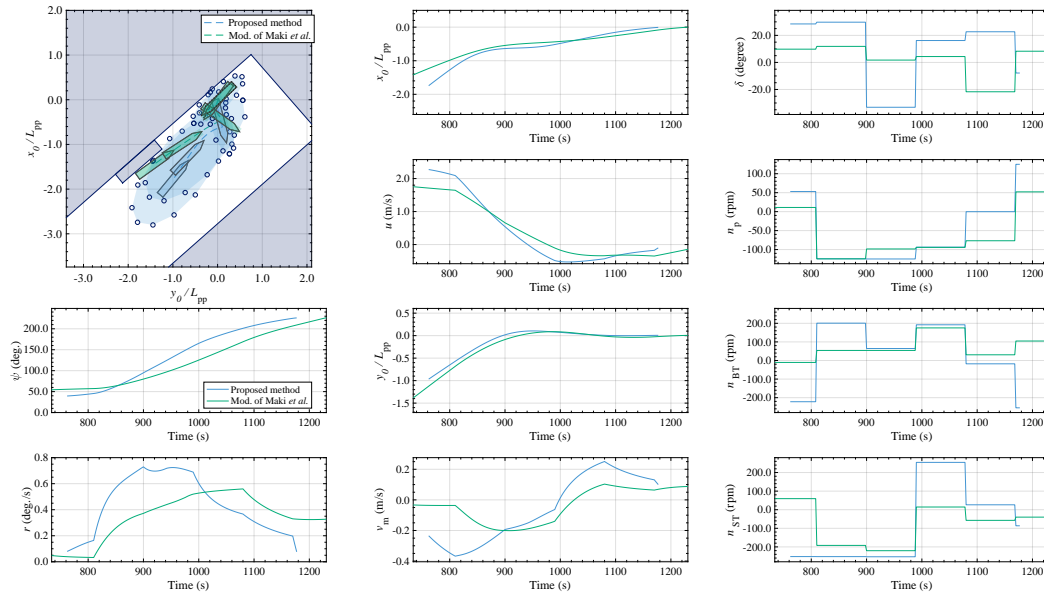


Fig. 9: Terminal phase of Fig.8 which of the Euclidean distance to berthing point is smaller than $2 L_{pp}$. Blue circles on the upper left figure are the collision avoidance points. The proposed method passed the moored vessel with distance while previous method passed without safety margin.

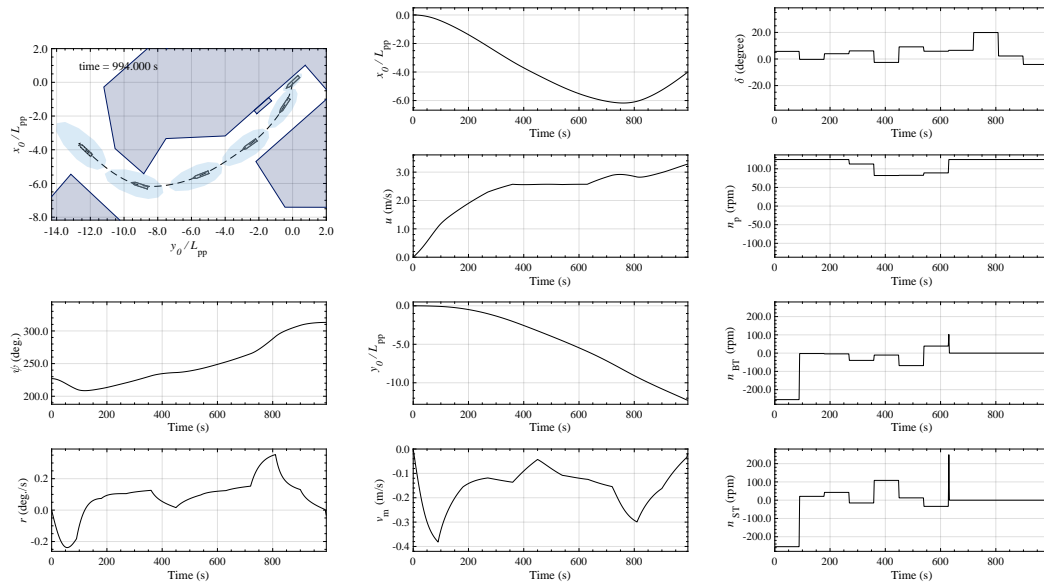


Fig. 10: Optimal control inputs and achieved state of unberthing on port of *Nanko*. Ellipse shown in light blue on figure of trajectory at upper left is the ship domain used in collision avoidance algorithm.

$$L_{WP,i} = \min \left(\sqrt{\{x_0(t) - x_{WP,i}\}^2 + \{y_0(t) - y_{WP,i}\}^2} \right). \quad (25)$$

Here, n_{WP} is the total number of way point, $x_{WP,i}$, $y_{WP,i}$ are the x_0 and y_0 coordinate of i -th waypoint, and $L_{WP,i}$ is the minimum distance between path of midship for i -th waypoint, respectively. L_{tol} is the tolerance distance from way point, same as x_{tol} . In this study, L_{tol} was set to $0.5 L_{pp}$.

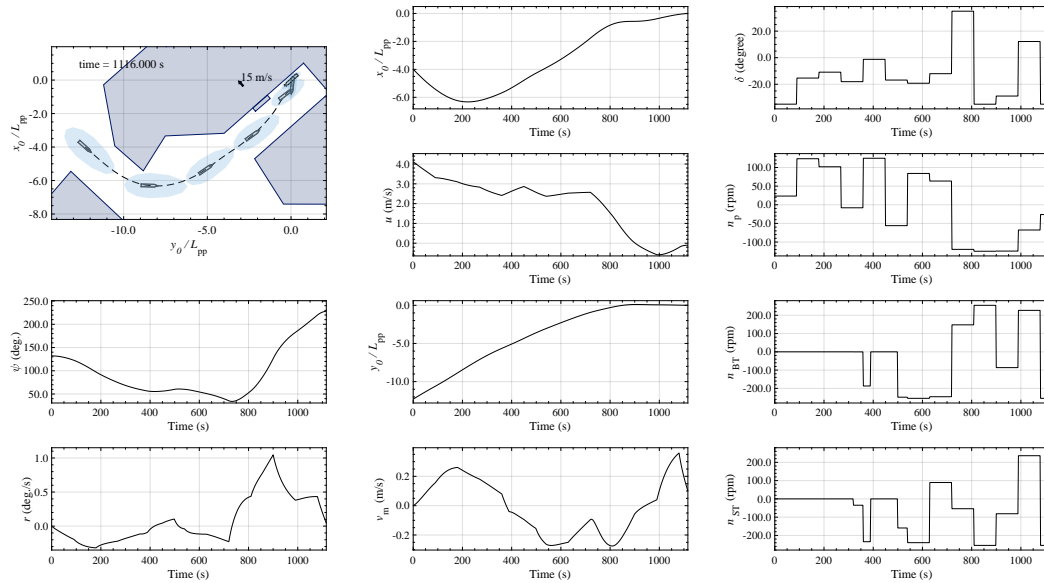


Fig. 11: Optimal control inputs and achieved state of berthing on port of *Nanko*. Computation with wind disturbance $U_T = 15$ m/s. Ellipse shown in light blue on figure of trajectory at upper left is the ship domain used in collision avoidance algorithm, and arrow at upper left figure indicates wind direction.

On the optimization with waypoints and new objective function Eq. (22), we tested with two waypoints $n_{WP} = 2$ on the berthing at the port of *Nanko*. Ideas of the selection of waypoints are as follows. First, waypoints are intended to generate a favorable gradient on J . We assumed that only a few waypoints were necessary to generate gradients, and designation of many waypoints undermines the automation of trajectory planning. Hence, the minimum number of waypoints ($n_{WP} = 2$), which can prove that the proposed method can handle multiple points, was chosen. Second, the location of waypoints was chosen to provide a guide point of a reasonable path. Locations of waypoints are shown in Fig. 16. The first waypoint was set at the harbor entrance, identical to the start point shown in Fig. 5. Another waypoint was set at the entrance of the confined berth. By setting waypoints as a guide point of the reasonable path, CMA-ES tries to generate the solution which likely to pass nearby the waypoints. Hence it increases the likelihood of obtaining the preferable solution.

The start point of the berthing with waypoints was set at the passage outside the breakwater, shown on Fig.16, which is identical to the computation can not obtain proper solution without waypoint (Fig. 15). Details of initial condition are as follows:

$$\mathbf{x}_{\text{int}} = (-753.7 \text{ m}, 8.0 \text{ kn}, -2892.1 \text{ m}, 0.0 \text{ m/s}, 45^\circ, 0.0^\circ/\text{s})^T \quad (26)$$

Computation results with waypoint are shown in Fig.17. By introducing waypoints and objective function with it, trajectory planning succeeded in which the ship arrived at the

designated berthing point and properly tracing the waypoint.

4. Discussion

As shown in the previous section, the proposed method can obtain collision-free, optimal trajectory and control input on real port geometry. Although the previous work of proposed method (Maki et al., 2020a,b) was not able to incorporate complex spatial constraints and not considered the wind disturbance, the present paper showed the improvement to overcome those limitations. We show applications become possible by the improvement later on in this section. Our proposed method can directly apply to the arbitrary spatial constraints while similar research mentioned in section 1.1 (Martinsen et al., 2021; Bitar et al., 2020; Bergman et al., 2020) have adopted the two-stage method; discrete the continuous state space to apply graph search which obtains an initial guess. The present method can handle the comprehensive ship's dynamics as single-stage optimization while graph search method can only address purely geometric space or limited way of ship dynamics. In addition, the present method varies the ship domain with speed which is natural for navigators' sense, while similar research (Bitar et al., 2020; Bergman et al., 2020) have only adopted to circular safety region around the ship with a constant region size.

Obtained trajectory and control can serve as a reference to the tracking control of berthing. On the optimization of real-time control method with finite prediction horizon, such as model predictive control (Li et al., 2020), those method could be unstable when the prediction horizon gets longer.

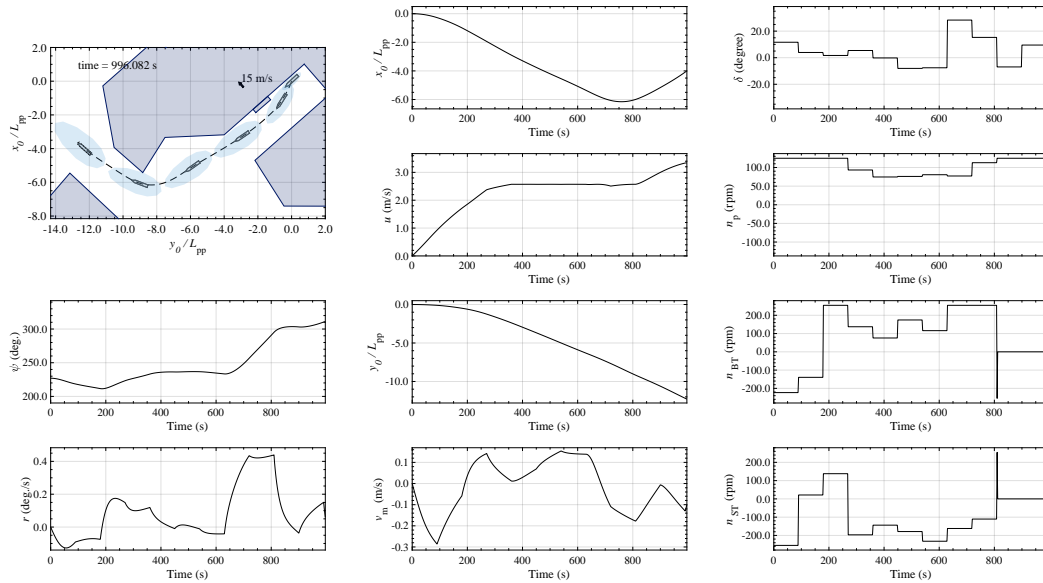


Fig. 12: Optimal control inputs and achieved state of unberthing on port of *Nanko*. Computation with wind disturbance $U_T = 15$ m/s. Ellipse shown in light blue on figure of trajectory at upper left is the ship domain used in collision avoidance algorithm, and arrow at upper left figure indicates wind direction.

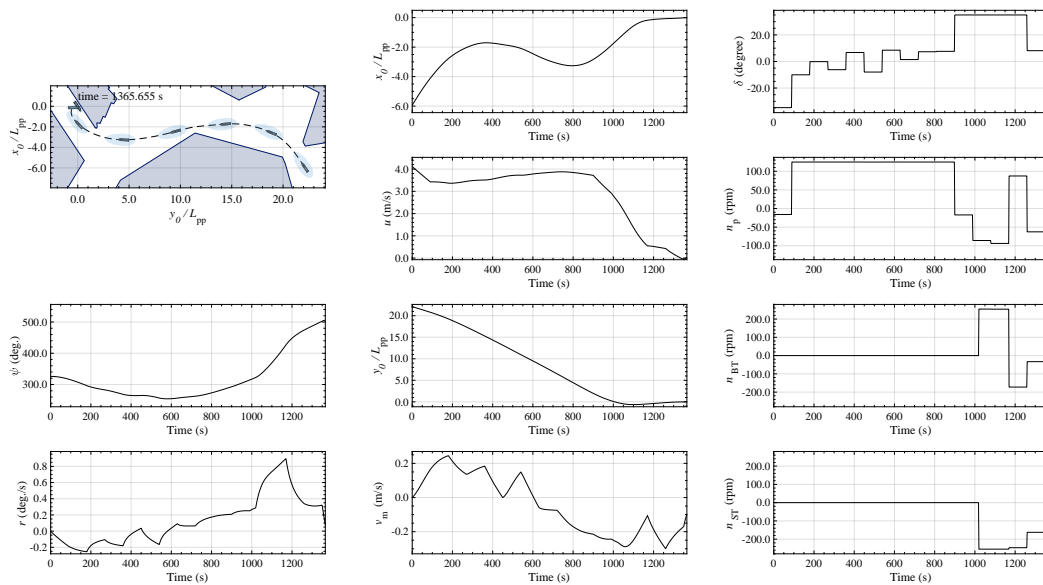


Fig. 13: Optimal control inputs and achieved state of berthing on port of *Ariake*. Computation without the wind disturbance. Ellipse shown in light blue on figure of trajectory at upper left is the ship domain used in collision avoidance algorithm

However, by offering predefined trajectory as a reference, prediction horizon can be taken shorter. Trajectory obtained by the proposed method is suitable for reference because it is time-optimized collision-free trajectory.

Moreover, the proposed method can also use to estimate

the limit of actuator capability. By exploring the maximum wind velocity which could maintain collision-free trajectory on certain actuator configuration and port geometry, the ship designer can evaluate current design is sufficient to satisfy operation requirement or not. For example, results on

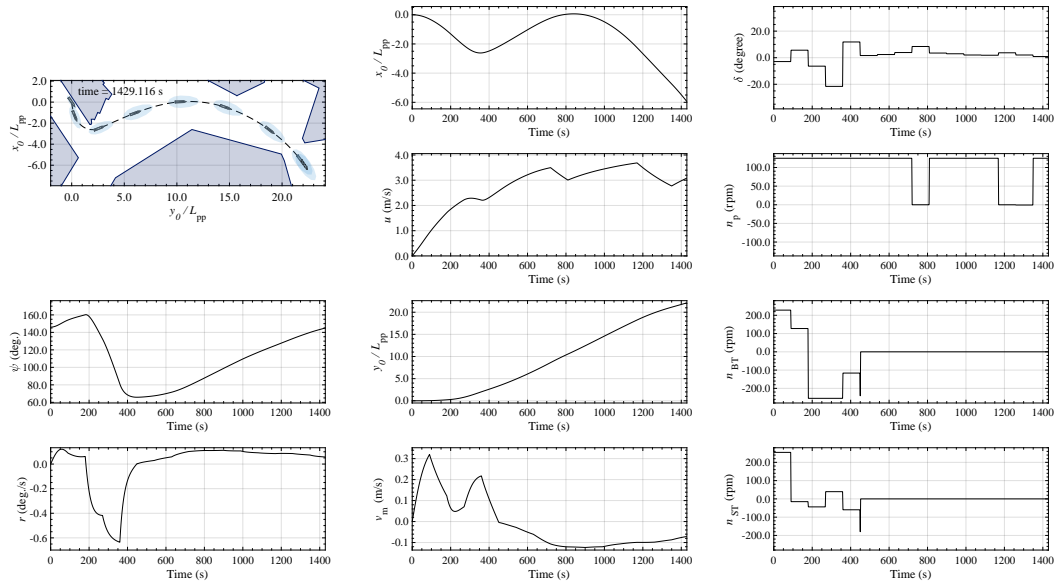


Fig. 14: Optimal control inputs and achieved state of unberthing on port of *Ariake*. Computation without the wind disturbance.

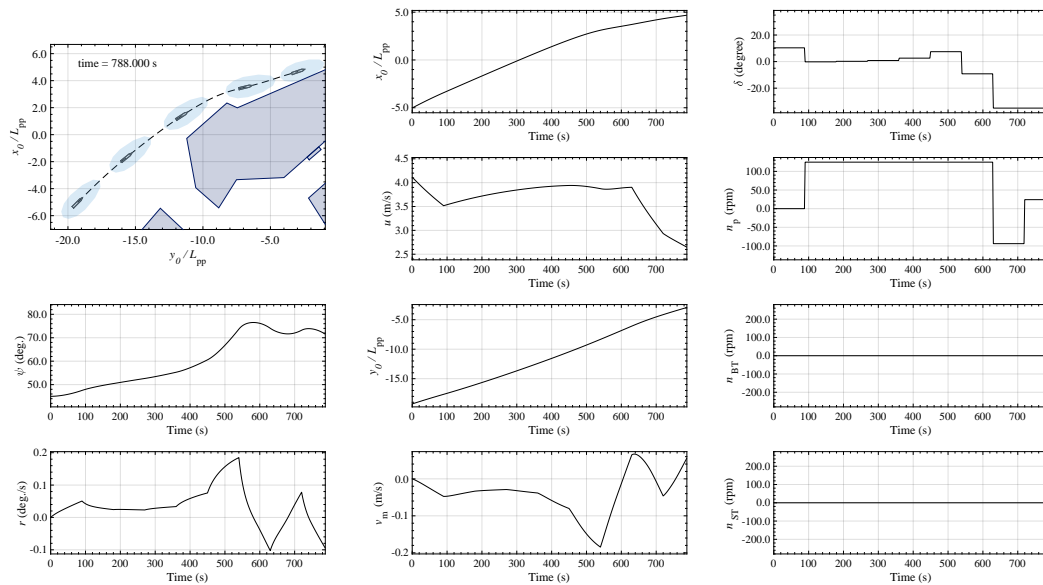


Fig. 15: Example of unfavorable solution at *Nanko*. The trajectory did not enter the opening of breakwater to enter the berth.

Section 3.3 shows that subject ship's design can berth and unberth under the wind condition of $\omega = (137^\circ, 15 \text{ m/s})$, while originally the maximum of side thruster's thrust was set to be equal to the wind pressure of 30 m/s lateral wind. However, the operational limit might be lower than 30 m/s, because the ship has to maneuver inside the spatial constraint of port geometry. We will be able to find nominal opera-

tional limit by increasing the wind condition from 15 m/s and find the maximum of the present method can find the collision-free trajectory.

The major drawback is its computational requirement. The proposed method can not directly apply to the real-time berthing control because of the computational requirement of the optimization process, which is due to the iteration.



Fig. 16: way point of port of Nanko

The proposed method takes few days for optimization. However, the proposed method can shorten its computational time requirement by applying parallel computation. CMA-ES uses multiple candidate solutions for a single iteration, as shown in Fig. 3, so each candidate solution's computation on objective function can easily parallelize. In addition, because of the computational requirement, we intended to use the proposed method combined with real-time control method as stated in the previous paragraph.

Major remaining issue is that the proposed method is not suitable for collision avoidance with the passing ships. Theoretically, the proposed method can search for a collision-free trajectory if the trajectory of the dynamic obstacle was predetermined. However, this computation would contribute little to autonomous berthing because on autonomous navigation, it is better to assume the passing ship's motion has some uncertainty. To overcome those drawbacks, The authors proposed using the current method to generate reference trajectory without passing ship, and the proposed method must be integrated with real-time control method for avoidance of passing ship. This issue is a future work for proposed method.

Another remaining issue of the proposed study is the treatment of unsteady wind disturbance. In this study, only steady wind disturbance was considered. As with the collision avoidance with passing ships, wind fluctuation must be overcome by integrating with the real-time control method.

Regarding the other potential future work, by improving two essential factors of trajectory planning, our work can add value as a reference trajectory; safety and optimization. From the safety perspective, the mathematical model of ship maneuver was assumed accurate enough. However, mathematical modeling of berthing maneuver itself still remains as research topic due to: the complexity and non-linearity of berthing motion; scale effect on hydrodynamic coefficients; and effect of shallow water and a sidewall. To negotiate the uncertainty of motion estimation caused by those factors, the robust optimization method is one option for improvement, other than improving the mathematical model itself by utilizing Computational fluid dynamics or model experiments

(Ueno and Tsukada, 2015; Ueno et al., 2017; Chen et al., 2021). In robust optimization, the range of possible range of uncertainly on input data is set in advance, and optimization is performed on the input data, which gives the worst result (Ben-Tal et al., 2009). From the optimization perspective, on the other hand, the practical berthing process is not just a single objective problem of time; optimization of berthing is a multi-objective optimization problem with the trade-off between time, energy consumption, and ride quality especially for passenger vessels. It is better to consider optimizing the berthing (and unberthing) trajectory as a multi-objective optimization problem that minimizes several factors simultaneously.

5. Conclusion

To achieve optimization of trajectory planning of berthing and unberthing of a ship at a real port, it is necessary to consider the spatial constraints, such as berths, breakwaters, buoys, or anchoring vessels. The novel collision avoidance algorithm was proposed, representing the spatial obstacles as polygons and includes a ship domain to maintain the sufficient distance to obstacles. The proposed ship domain consists of domain boundary vertices that discretize the ellipse shape of the ship domain with a uniform argument angle, and the size of the ship domain changes with ship's speed, which is based on the navigators' knowledge and experience.

Optimization of trajectory planning for two existing ports, *Nanko* and *Ariake*, were conducted by using the proposed collision avoidance algorithm with CMA-ES and the MMG model. By introducing the proposed collision avoidance algorithm, collision-free time-optimal control inputs and trajectories were obtained. The effect of wind disturbance was also considered. By considering the wind force, the obtained trajectory will be more robust that considers the limits of actuators. Additionally, optimization with waypoints also shown in this study. Including the waypoints to objective function makes it more robust to the choice of the initial location of berthing simulation. Although its long computation time due to the iteration, it should be noted that the present method requires only the mathematical model of ship maneuver, a start point, an end point, polygons of spatial constraints, and waypoints, if necessary, to obtain an optimal trajectory at the real port. The optimal trajectory can serve as a predefined reference to the real-time tracking control of berthing and unberthing.

CRedit authorship contribution statement

Yoshiki Miyauchi: Methodology, Software, Writing - original draft, visualization. **Ryohei Sawada:** Methodology, Writing - review & editing. **Youhei Akimoto:** Software, Writing - review & editing. **Naoya Umeda:** Supervision, Funding acquisition. **Atsuo Maki:** Conceptualization, Writing - review & editing.

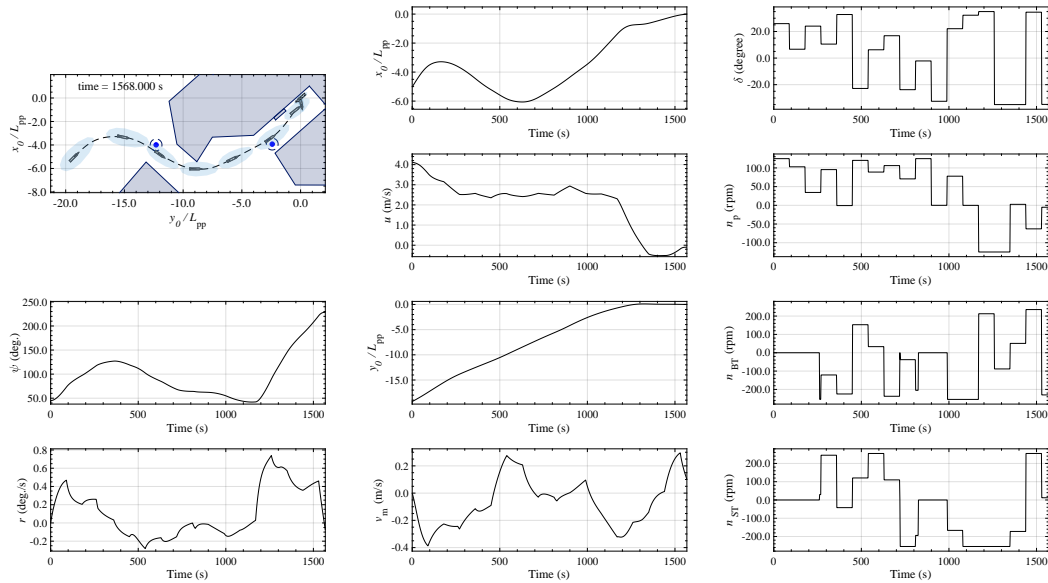


Fig. 17: Computation with way points at *Nanko*. blue dashed circle shows the way point with tolerance distance.

Declaration of competing interest

The authors declare that they have no known competing financial interests or personal relationships that could have appeared to influence the work reported in this paper.

Acknowledgment

This study was supported by a Grant-in-Aid for Scientific Research from the Japan Society for Promotion of Science (JSPS KAKENHI Grant #19K04858). The study also received assistance from JFY2018 Fundamental Research Developing Association for Shipbuilding and Offshore (REDAS) in Japan.

This is accepted manuscript. Published journal Article is shown on <https://doi.org/10.1016/j.oceaneng.2021.110390>.

A. Supplementary data

Supplementary data related to this article can be found at <https://doi.org/10.1016/j.oceaneng.2021.110390>.

References

- Ahmed, Y.A., 2015. Automatic Berthing Control Practically Applicable under Wind Disturbances. Ph.D. thesis. Osaka University.
- Amendola, J., Miura, L.S., Costa, A.H., Cozman, F.G., Tannuri, E.A., 2020. Navigation in restricted channels under environmental conditions: Fast-time simulation by asynchronous deep reinforcement learning. *IEEE Access* 8, 149199–149213. doi:10.1109/ACCESS.2020.3015661.
- Auger, A., Hansen, N., 2005. A restart cma evolution strategy with increasing population size, in: 2005 IEEE Congress on Evolutionary Computation, IEEE. pp. 1769–1776. URL: <http://ieeexplore.ieee.org/document/1554902/>, doi:10.1109/CEC.2005.1554902.
- Ben-Tal, A., Ghaoui, L., Nemirovski, A., 2009. Robust Optimization. Princeton Series in Applied Mathematics, Princeton University Press. URL: <https://books.google.co.jp/books?id=DttjR7IpjUEC>.
- Bergman, K., Ljungqvist, O., Linder, J., Axehill, D., 2020. An Optimization-Based Motion Planner for Autonomous Maneuvering of Marine Vessels in Complex Environments, in: 2020 59th IEEE Conference on Decision and Control (CDC), IEEE. pp. 5283–5290. URL: <https://ieeexplore.ieee.org/document/9303746/http://arxiv.org/abs/2012.12145>, doi:10.1109/CDC42340.2020.9303746, arXiv:2005.02674.
- Bitar, G., Martinsen, A.B., Lekkas, A.M., Breivik, M., 2020. Two-stage optimized trajectory planning for asvs under polygonal obstacle constraints: Theory and experiments. *IEEE Access* 8, 199953–199969. URL: <https://www.maritime-executive.com/article/rolls-royce-and-wartsila->, doi:10.1109/access.2020.3035256.
- Chen, G., Tu, J., Ti, X., Wang, Z., Hu, H., 2021. Hydrodynamic model of the beaver-like bendable webbed foot and paddling characteristics under different flow velocities. *Ocean Engineering* 234, 109179. URL: <https://www.sciencedirect.com/science/article/pii/S0029801821006120>, doi:https://doi.org/10.1016/j.oceaneng.2021.109179.
- Fujii, Y., Tanaka, K., 1971. Traffic capacity. *Journal of Navigation* 24, 543–552. URL: https://www.cambridge.org/core/product/identifier/S0373463300022384/type/journal_article, doi:10.1017/S0373463300022384.
- Fujiwara, T., Ueno, M., Nimura, T., 1998. Estimation of wind forces and moments acting on ships. *Journal of the Society of Naval Architects of Japan* 1998, 77–90. URL: <http://joi.jlc.jst.go.jp/JST.Journalarchive/jjasnaoe1968/1998.77?from=CrossRef>, doi:10.2534/jjasnaoe1968.1998.77.
- Goodwin, E.M., 1975. A statistical study of ship domains. *Journal of Navigation* 28, 328–344. doi:10.1017/S0373463300041230.
- Hachii, T., 2004. The prediction of manoeuvring motion on ships with low speed using standard MMG model. Master's thesis. Osaka University.
- Hansen, M.G., Jensen, T.K., Lehn-Schiøler, T., Melchior, K., Rasmussen, F.M., Ennemark, F., 2013. Empirical ship domain based on ais data. *Journal of Navigation* 66, 931–940. URL: https://www.cambridge.org/core/product/identifier/S0373463313000489/type/journal_article,

- doi:10.1017/S0373463313000489.
- Hansen, N., 2006. The CMA Evolution Strategy: A Comparing Review. Springer Berlin Heidelberg, Berlin, Heidelberg. pp. 75–102. URL: https://doi.org/10.1007/3-540-32494-1_4, doi:10.1007/3-540-32494-1_4.
- Hasegawa, K., Kitera, K., 1993. Mathematical model of manoeuvrability at low advance speed and its application to berthing control, in: 2nd Japan-Korea Joint Workshop on Ship and Marine Hydrodynamics, pp. 311–321.
- Inoue, K., Usami, S., Shibata, T., 1994. Modelling of mariners' senses on minimum passing distance between ships in harbour. The Journal of Japan Institute of Navigation 90, 297–306. doi:10.9749/jin.90.297.
- Jensen, T.K., Hansen, M.G., Lehn-Schiøler, T., Melchild, K., Rasmussen, F.M., Ennemark, F., 2013. Free flow–efficiency of a one-way traffic lane between two pylons. Journal of Navigation 66, 941–951. URL: <https://doi.org/10.1017/S0373463313000362>https://www.cambridge.org/core/product/identifier/S0373463313000362/type/journal_article, doi:10.1017/S0373463313000362.
- Kitagawa, Y., Tsukada, Y., Miyazaki, H., 2015. 2015s-gs1-1 a study on mathematical models of propeller and rudder under maneuvering with propeller reverse rotation. Conference Proceedings The Japan Society of Naval Architects and Ocean Engineers 20, 117–120. doi:10.14856/conf.20.0_117.
- Kobayashi, E., 1988. A simulation study on ship manoeuvrability at low speeds. Akishima Laboratory, Ocean Engineering Research Section, Mitsubishi Heave Industries Ltd. Published in: Mitsubishi Technical Bulletin No. 180.
- Kobayashi, E., 1990. Manoeuvring simulation at low speed for a ship with twin screw, rudders and thrusters. MARSIM and ICSM 90, Intl. Conference, Marine Simulation and Ship Manoeuvrability.
- Kobayashi, H., Blok, J., Barr, R., Kim, Y.S., Nowicki, J., 2002. The specialist committee on eso osaka final report and recommendations to the 23rd ittc. 23rd International Towing Tank Conference II, 581–743.
- Li, S., Liu, J., Negenborn, R.R., Wu, Q., 2020. Automatic Docking for Underactuated Ships Based on Multi-Objective Nonlinear Model Predictive Control. IEEE Access 8, 70044–70057. doi:10.1109/ACCESS.2020.2984812.
- Liu, J., Zhou, F., Li, Z., Wang, M., Liu, R.W., 2016. Dynamic Ship Domain Models for Capacity Analysis of Restricted Water Channels. Journal of Navigation 69, 481–503. URL: https://www.cambridge.org/core/product/identifier/S0373463315000764/type/journal_article, doi:10.1017/S0373463315000764.
- Maki, A., Akimoto, Y., Naoya, U., 2020a. Application of optimal control theory based on the evolution strategy (cma-es) to automatic berthing (part: 2). Journal of Marine Science and Technology (Japan) doi:10.1007/s00773-020-00774-x.
- Maki, A., Sakamoto, N., Akimoto, Y., Nishikawa, H., Umeda, N., 2020b. Application of optimal control theory based on the evolution strategy (cma-es) to automatic berthing. Journal of Marine Science and Technology 25, 221–233. URL: <https://doi.org/10.1007/s00773-019-00642-3><http://link.springer.com/10.1007/s00773-019-00642-3>, doi:10.1007/s00773-019-00642-3.
- Martinsen, A.B., Lekkas, A.M., Gros, S., 2019. Autonomous docking using direct optimal control. IFAC-PapersOnLine 52, 97–102. doi:10.1016/j.ifacol.2019.12.290.
- Martinsen, A.B., Lekkas, A.M., Gros, S., 2021. Optimal model-based trajectory planning with static polygonal constraints. IEEE Transactions on Control Systems Technology, 1–12doi:10.1109/TCST.2021.3094617.
- Miyauchi, Y., Maki, A., Umeda, N., Rachman, D.M., Akimoto, Y., 2021. System parameter exploration of ship maneuvering model for automatic docking / berthing using cma-es. arXiv preprint, URL: <https://arxiv.org/abs/2111.06124>.
- Murakami, K., Takenobu, M., Miyata, T., Yoneyama, H., 2015. Fundamental Analysis on the Characteristics of Berthing Velocity of Ships For the Design of Port Facilities. Technical Report. TECHNICAL NOTE of National Institute for Land and Infrastructure Management.
- Ogawa, A., Kasai, H., 1978. On the mathematical model of manoeuvring motion of ships. International Shipbuilding Progress 25, 306–319. doi:10.3233/ISP-1978-2529202.
- Pietrzykowski, Z., 2008. Ship's fuzzy domain – a criterion for navigational safety in narrow fairways. Journal of Navigation 61, 499–514. URL: https://www.cambridge.org/core/product/identifier/S0373463308004682/type/journal_article, doi:10.1017/S0373463308004682.
- Roubos, A., Groenewegen, L., Peters, D.J., 2017. Berthing velocity of large seagoing vessels in the port of rotterdam. Marine Structures 51, 202–219. doi:10.1016/j.marstruc.2016.10.011.
- Sakamoto, N., Akimoto, Y., 2017. Modified box constraint handling for the covariance matrix adaptation evolution strategy, in: Proceedings of the Genetic and Evolutionary Computation Conference Companion, Association for Computing Machinery, New York, NY, USA. p. 183–184. URL: <https://doi.org/10.1145/3067695.3075986>, doi:10.1145/3067695.3075986.
- Serigstad, E., Eriksen, B.O.H., Breivik, M., 2018. Hybrid collision avoidance for autonomous surface vehicles. IFAC-PapersOnLine 51, 1–7. URL: <https://linkinghub.elsevier.com/retrieve/pii/S2405896318321499>, doi:10.1016/j.ifacol.2018.09.460.
- Seta, H., Inoue, K., USsui, H., 2004. Supporting information for safe ship handling based on the concept of potential area of water. The Journal of Japan Institute of Navigation 111, 63–69. URL: https://www.jstage.jst.go.jp/article/jin/111/0/111_KJ00004696699/_article/-char/ja, doi:10.9749/jin.111.63.
- Szlapczynski, R., Szlapczynska, J., 2017. Review of ship safety domains: Models and applications. Ocean Engineering 145, 277–289. doi:10.1016/j.oceaneng.2017.09.020.
- The Harbor Information Center for the Security of Ship Navigation, 2020. Port of Osaka Entrance and Departure Manual. Revised ed., Osaka ports and harbors bureau.
- Ueno, M., Nimura, T., Miyazaki, H., Fujiwara, T., Nonaka, K., Yabuki, H., 2001. Model experiment and sea trial for investigating manoeuvrability of a training ship. Journal of the Society of Naval Architects of Japan 2001, 71–80. URL: <http://joi.jlc.jst.go.jp/JST.Journalarchive/jjasnaoe1968/2001.71?from=CrossRef>, doi:10.2534/jjasnaoe1968.2001.71.
- Ueno, M., Suzuki, R., Tsukada, Y., 2017. Estimation of stopping ability of full-scale ship using free-running model. Ocean Engineering 130, 260–273. URL: <https://www.sciencedirect.com/science/article/pii/S0029801816305819>, doi:https://doi.org/10.1016/j.oceaneng.2016.12.001.
- Ueno, M., Tsukada, Y., 2015. Rudder effectiveness and speed correction for scale model ship testing. Ocean Engineering 109, 495–506. URL: <https://www.sciencedirect.com/science/article/pii/S0029801815005132>, doi:https://doi.org/10.1016/j.oceaneng.2015.09.041.
- Vagale, A., Oucheikh, R., Bye, R.T., Osen, O.L., Fossen, T.I., Oucheikh, R., Osen, O.L., Fossen, T.I., 2021. Path planning and collision avoidance for autonomous surface vehicles I: a review. Journal of Marine Science and Technology URL: <https://doi.org/10.1007/s00773-020-00787-6><http://link.springer.com/10.1007/s00773-020-00787-6>, doi:10.1007/s00773-020-00787-6.
- Wang, Y., Chin, H.C., 2016. An empirically-calibrated ship domain as a safety criterion for navigation in confined waters. Journal of Navigation 69, 257–276. URL: https://www.cambridge.org/core/product/identifier/S0373463315000533/type/journal_article, doi:10.1017/S0373463315000533.
- Yamanouchi, H., Fujii, Y., 1972. On the hard core of the effective domain in yokohama port. NAVIGATION 38, 56–57. doi:10.18949/jinnavig.38.0_56.
- Yasukawa, H., Yoshimura, Y., 2015. Introduction of mmg standard method for ship maneuvering predictions. Journal of Marine Science and Technology (Japan) 20, 37–52. doi:10.1007/s00773-014-0293-y.
- Yoshimura, Y., Nakao, I., Ishibashi, A., 2009. Unified mathematical model for ocean and harbour manoeuvring, in: Proceedings of MARSIM2009, pp. 116–124. URL: <http://hdl.handle.net/2115/42969>.